

## Exponential Size Distribution of von Willebrand Factor

Svenja Lippok,<sup>†</sup> Tobias Obser,<sup>‡</sup> Jochen P. Müller,<sup>§</sup> Valentin K. Stierle,<sup>†</sup> Martin Benoit,<sup>§</sup> Ulrich Budde,<sup>¶</sup> Reinhard Schneppenheim,<sup>‡</sup> and Joachim O. Rädler<sup>†\*</sup>

<sup>†</sup>Faculty of Physics and Center for NanoScience, Ludwig Maximilian University, Munich, Germany; <sup>‡</sup>Department of Pediatric Hematology and Oncology, University Medical Center, Hamburg-Eppendorf, Hamburg, Germany; <sup>§</sup>Chair for Applied Physics, Ludwig Maximilian University, Munich, Germany; and <sup>¶</sup>Coagulation Lab, AescuLabor Hamburg, Hamburg, Germany

**ABSTRACT** Von Willebrand Factor (VWF) is a multimeric protein crucial for hemostasis. Under shear flow, it acts as a mechanosensor responding with a size-dependent globule-stretch transition to increasing shear rates. Here, we quantify for the first time, to our knowledge, the size distribution of recombinant VWF and VWF-eGFP using a multilateral approach that involves quantitative gel analysis, fluorescence correlation spectroscopy, and total internal reflection fluorescence microscopy. We find an exponentially decaying size distribution of multimers for recombinant VWF as well as for VWF derived from blood samples in accordance with the notion of a step-growth polymerization process during VWF biosynthesis. The distribution is solely described by the extent of polymerization, which was found to be reduced in the case of the pathologically relevant mutant VWF-IIC. The VWF-specific protease ADAMTS13 systematically shifts the VWF size distribution toward smaller sizes. This dynamic evolution is monitored using fluorescence correlation spectroscopy and compared to a computer simulation of a random cleavage process relating ADAMTS13 concentration to the degree of VWF breakdown. Quantitative assessment of VWF size distribution in terms of an exponential might prove to be useful both as a valuable biophysical characterization and as a possible disease indicator for clinical applications.

### INTRODUCTION

The large plasma glycoprotein von Willebrand Factor (VWF) is essential for the initiation of blood coagulation as it promotes adhesion of platelets to the injured vessel wall as well as platelet aggregation (1,2). It is present in human blood and the secretory granules of endothelial cells and platelets. Plasma VWF plays a crucial role in early hemostasis as it binds rapidly and tightly to collagen whenever blood is exposed to injured tissues (3). Remarkably, VWF is a multimer that consists of several identical subunits and its function in primary hemostasis strictly correlates with its multimer size. Even though much research is being done on its size-dependent functionality, only little is known about the exact size distribution and its origin. Quantitative deficiency of plasma VWF causes von Willebrand disease (VWD) type 1, the most common congenital bleeding disorder (1). Although VWD is often caused by a lack of long multimers, an aberrantly increased activity of VWF due to larger than normal multimers is assumed to be a pathogenic factor in thrombotic thrombocytopenic purpura (2,4). The size-dependent functionality relates to the shear flow-sensitive structure of VWF, which responds to shear by expansion to an elongated form, thereby exposing binding sites for collagen and the platelet receptor GPIb (5). This process highly depends on the extent of multimerization of VWF because smaller multimers are more resistant to shear forces than larger ones and subsequently binding sites for their ligands are not as readily exposed (6,7). Consequently, the

size of the multimeric VWF is a critical factor for VWF's functionality and the question arises, which size distribution is produced by VWF biosynthesis and how it is controlled in homeostasis. In polymer science, the problem of polymer size distribution has been addressed by the seminal work of Paul Flory in 1936, in which he calculated the exact size distribution of polymers based on the model of step-growth polymerization reaction (8). He showed that a theoretical prediction of a multimer size distribution is possible if the mechanism and the kinetics of the synthesis reaction are known. Vice versa, the size distribution provides clues with respect to the polymerization mechanism.

VWF is expressed as a propeptide (Fig. 1 A), which is translocated into the endoplasmatic reticulum, where it dimerizes via intermonomer disulfide bonds in the C-terminal domain (Fig. 1 B). The dimers with a molecular mass of 500 kDa represent the repeating unit of the VWF multimer. They are transported from the endoplasmatic reticulum (pH  $\approx$  7.4) to the Golgi (pH  $\approx$  6.2). This is the place where multimerization occurs by formation of linear multimers via interchain disulfide bonds at the N-terminal resulting in multimeric VWF with molecular masses of up to  $>$  40.000 kDa (Fig. 1 C) (9–11). In this process, VWF propeptide acts as an oxidoreductase to promote VWF multimerization (12–14). The propeptide is then cleaved for separate secretion (15,16). After multimerization, VWF is either secreted constitutively to the plasma or stored in Weibel-Palade bodies and released upon certain stimuli (e.g., thrombin, plasmin, fibrin) without further multimerization taking place in the plasma (17). For a postsecretion size regulation, circulating VWF undergoes cleavage by

Submitted April 3, 2013, and accepted for publication July 24, 2013.

\*Correspondence: raedler@lmu.de

Editor: Ashok Deniz.

© 2013 by the Biophysical Society  
0006-3495/13/09/1208/9 \$2.00

<http://dx.doi.org/10.1016/j.bpj.2013.07.037>



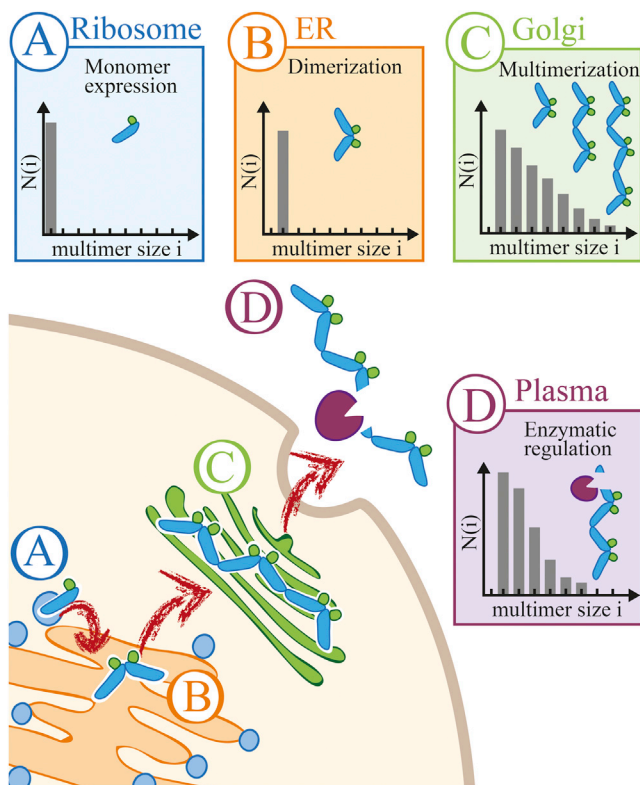


FIGURE 1 Schematic representation of plasma VWF size regulation. (A) VWF is synthesized by endothelial cells and megakaryocytes and originates from a 360 kDa monomer. (B) Monomeric VWF is transported to the endoplasmic reticulum where it is dimerized through intermonomer disulfide bonds. (C) Multimerization takes place in the Golgi apparatus, where the dimers form multimers with sizes ranging from 500 to 40,000 kDa, which are then secreted to the blood plasma. (D) Size control in plasma is provided by the protease ADAMTS13. No further multimerization occurs after secretion to the plasma.

the specific metalloprotease ADAMTS13, a disintegrin and metalloproteinase with a thrombospondin type 1 motif, member 13 (Fig. 1 D) (18). As known from bleeding disorders, defects in VWF multimer synthesis or size regulation have fundamental implications in hemostasis and exhibit defined patterns in VWF gel electrophoresis. Yet, the size distribution of VWF and its molecular causation has not been quantitatively studied so far.

Here, we investigate the size distribution of VWF using fluorescence correlation spectroscopy (FCS), quantitative gel analysis, and total internal reflection fluorescence microscopy (TIRFM). TIRFM allows for direct imaging of recombinant VWF-eGFP multimers including the assessment of VWF size by intensity analysis. Gel analysis is widely accepted in VWF diagnostics for screening patient samples for diseases. FCS measures the hydrodynamic size of fluorescently labeled species in solution. In contrast to gel analysis and TIRFM, FCS allows for measurements of fluorescent VWF-eGFP in blood plasma and is therefore well suited for VWF analysis in its native environment. We compare the size distribution of recombinant VWF

and VWF-eGFP and its disease-related mutant VWF 2A (IIC), which is characterized by an increased concentration of dimers (19,20). We show that after secretion from VWF producing cells, VWF has an exponential size distribution in both healthy and pathologic form. The physiological and pathological distributions are distinct in the extent of polymerization characterizing the distribution. We also show that proteolytic cleavage by ADAMTS13 leads to non-exponential distributions that shift with time allowing for in situ monitoring of VWF cleavage under blood plasma conditions.

## MATERIALS AND METHODS

### Production of recombinant VWF

The recombinant fusion protein rVWF-eGFP was expressed and purified separately in its monomer, dimer, and multimer form as described in detail in the following:

#### Cloning of a VWF-enhanced green fluorescent protein (EGFP) Plasmid

From the plasmid pIRESneo2-vWF (Takara Bio Europe/Clontech, Saint-Germain-en-Laye, France) the stop codon was eliminated and an *EcoRI* restriction site was introduced. The EGFP sequence was cut out from the plasmid pEGFP-N2 (Takara Bio Europe/Clontech) by *EcoRI* and *NotI* and inserted into plasmid pIRESneo2 by using its *EcoRI/NotI* restriction sites (pIRESneo2-EGFP). Subsequently, VWF-cDNA from plasmid pIRESneo2-VWF lacking the stop codon was cut out by *EcoRI* and cloned into pIRESneo2-EGFP (pIRESneo2-VWF-EGFP).

pIRESneo2-VWF-EGFP was then used to produce three mutant constructs:

- 1) pIRESneo2-vWF-delPro-EGFP with the retained signal peptide sequence and the first three codons of the VWF propeptide but lacking the rest of the propeptide corresponding to codons 26–763 (delT26–R763). Expression of this construct will result in VWF monomers that assemble into carboxy-terminal dimers but not into larger multimers.
- 2) pIRESneo2-vWF-delPro/C2771R-EGFP, which was produced by in vitro-mutagenesis of construct 1), by exchanging codon 2771 for cysteine against the naturally occurring mutation to arginine (p.C2771R). Expression of this construct results in VWF monomers only, because p.C2771R causes a severe dimerization defect (R. Schneppenheim, unpublished) in addition to the multimerization defect of the VWF-delPro construct 1).
- 3) pIRESneo2-vWF-C1099Y-EGFP, which was produced by in vitro-mutagenesis of wild-type pIRESneo2-VWF-EGFP, by exchanging codon 1099 for cysteine against the naturally occurring mutation to tyrosine (p.C1099Y). Expression of this mutant results in near normal quantitative expression of mutant VWF, however, lacking large and medium sized VWF multimers as in the phenotype IIC of VWD type 2A.

#### Generation of stable cell lines constitutively secreting VWF

Transfection of 293 cells was carried out as described previously (21). 48 h after transfection cells were trypsinized and grown until confluence in Dulbecco's modified Eagle's medium buffer containing 10% fetal bovine serum and G418 at 500  $\mu\text{g/ml}$  for selection. After further propagation of an aliquot of the stable cell line until 70–80% confluence, cell culture medium was changed to OPTIPRO-SFM medium for serum-free expression. Cell culture medium was harvested after 72 h and concentrated by Amicon Ultrafree (MWC0 100000 DA) if necessary.

## Blood samples

The patient samples were sent to our laboratory for the evaluation of VWF multimers and subtyping of the already known VWD. Informed consent was obtained from all subjects.

## Quantitative gel analysis

VWF multimer analysis was carried out in sodium dodecyl sulfate agarose gels combined with immunoblotting and luminescence visualization. The luminescent blot was stored on electronic media using photo imaging (FluorChem8000; Alpha Innotech, San Leandro, CA) (22). VWF multimers were separated via gel electrophoresis and visualized by detecting their luminescent signal. Electrophoretic bands were visualized by means of luminescent immunoblotting. Thereby, intensities were obtained by labeling the proteins with horseradish peroxidase-conjugated antibodies that cleave a chemiluminescent agent producing luminescence that is proportional to the amount of protein (23).

The multimer patterns of rVWF and rVWF-eGFP are taken from different gels, which were recorded on different days. Therefore, the run times vary from sample to sample. As the run times are not used for data analysis this does not have any influence on the analyzed data.

## FCS

FCS detects the dynamics of fluorescently labeled molecules diffusing in and out of a confocal volume (24–28) and can be applied to multicomponent systems with different fluorescent species (29). It can be used for measurements in crowded media like blood plasma, thus enabling the study of molecules in their native environment (30). This ensures that the investigated molecules keep their natural properties, because these often change in bulk fluids acting as solvents and thereby reducing effects such as aggregation. FCS data analysis is described in detail in the [Supporting Material](#).

For FCS measurements, an Axiovert 200 microscope with a ConfoCor 2 unit (Carl Zeiss, Jena, Germany) equipped with a 40× (NA = 1.2) water immersion apochromat objective (Carl Zeiss) was used. An argon laser (488 nm) was used for illumination. Samples were measured in eight-well LabTek I chamber slides (Nunc, Rochester, NY). All measurements were performed in 5 mM Tris-HCl, pH 8.0 with 1.5 M urea at a temperature of 37°C controlled by an ibidi heating stage (ibidi GmbH, Martinsried, Germany). At this urea concentration, VWF can be conceived as a semi-flexible polymer as urea stretches it without affecting its basic structure. These conditions are widely used for VWF analysis if measurements with the stretched polymer have to be performed without shear flow (4,31). eGFP functionality was proved to be functional under this buffer condition in agreement with Alkaabi et al. (32). Measurements were performed for 10 × 60 s (eGFP, monomer and dimer) and 20 × 6 min (rVWF; rVWF-IIC). To ensure optimal fluctuation detection for multicomponent analysis, we chose long measurement times to obtain sufficient statistics while keeping concentrations low (20 nM for all samples). Correlation was performed using ConfoCor 2 software. For FCS data analysis, a Labview routine was implemented.

## TIRFM

TIRFM is a suitable technique for imaging fluorescent molecules on a transparent substrate with single molecule resolution (33,34). The technique uses the evanescent field of a totally internal reflected laser beam exciting only fluorophores above the substrate surface within typically 100 nm. This provides a high signal/noise ratio of the collected fluorescence and is therefore well suited for direct imaging of fluorescent molecules.

For TIRFM measurements, rVWF was immobilized on epoxy silane-coated glass slides and imaged using the TIRFM setup presented in (35).

For excitation in the total internal reflection mode, a 473 nm laser (iBeam smart, TOPTICA, Gräfelfing, Germany) was used at a power of 0.4 mW. The corresponding filter set consisted of a Chroma z 470/10, a Chroma z 470 RDC, and a Chroma HQ 525/50 (Chroma Technology GmbH, Olching, Germany). The emitted light signal was detected by a back-illuminated EMCCD camera (DU-860D, Andor, Belfast, Ireland). The EMCCD chip was operated at a temperature of −90°C and the electron multiplication gain was set to 300-fold. 3000 frames (21 × 21 μm<sup>2</sup>) were taken per image sequence with a recording rate of 10 frames/s. All measurements were carried out in phosphate buffered saline. To minimize eGFP bleaching before the actual measurement, all adjustment procedures were carried out at low laser power (0.1 mW).

Data analysis was obtained with a step detection algorithm. As the routine cannot distinguish between on- and off-steps and fails in detecting steps that occur within a very short time slot, the obtained step number was corrected by eye for blinking and missed steps.

## Proteolysis of full-length rVWF by ADAMTS13

Cleavage of recombinant VWF-eGFP by ADAMTS13 was achieved as reported in Pruss et al. (36). Cleaved samples were stored at −80°C until multimer analysis was performed.

## RESULTS

### Quantitative gel analysis of rVWF

Gel analysis is the most frequently used technique for VWF multimer analysis (22,23,36). By quantitative analysis of the intensity profiles obtained by antibody staining in gels (Fig. 2, A,B and C,D, respectively) we yield the size distribution of VWF, which in a semilogarithmic plot shows good agreement with an exponential (Fig. 2, E and F). Hereby we assume that antibody staining is proportional to the number of dimers in the VWF multimer. The gels were evaluated using luminescent immunoblotting implying that the measured luminescent signal intensities in each band reflect the number of antibody labels (Fig. 2, C and D). The signal was normalized by the number of dimers  $i$  corresponding to the size of the multimers in the respective band. These normalized intensities correspond to the molar distribution function and were plotted in a semilogarithmic diagram versus the multimer size given in number of dimers  $i$  (Fig. 2, E and F). We took gel data from both wild-type rVWF and rVWF-IIC and their eGFP fusion analogs (Fig. 2 A) as well as from VWF of normal plasma VWF-NP and patient plasma VWF-IIC (Fig. 2 B). For rVWF, clearly an exponential decay is found. One possible mechanistic explanation for such an exponential decay is the Flory theory of linear condensation polymers (8) that describes a step-growth polymerization process taking place in an enclosed reactor by the intermolecular reaction of bifunctional compounds (for details, see the [Supporting Material](#)). It predicts an exponential size distribution for step-growth polymerization resulting in a molar fraction of  $i$ -mers containing  $i$  subunits (8)

$$\frac{N_i}{N} = (1 - p)p^{i-1}. \quad (1)$$

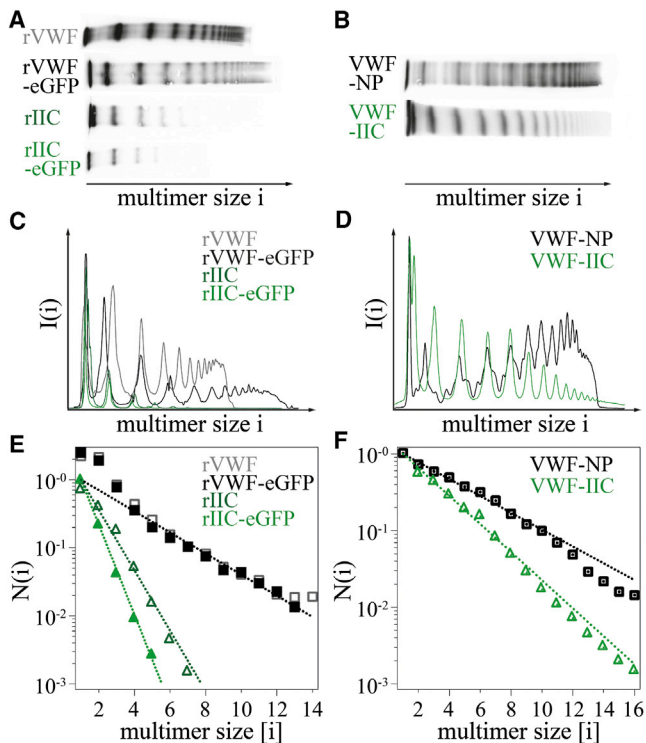


**FIGURE 2** Quantitative gel analysis of recombinant and blood plasma VWF. (A) Multimer patterns of recombinant VWF distributions showing a ladder of multimers. (B) Multimer patterns of VWF distribution of normal plasma and of a patient with von Willebrand disease type IIC. (C and D) Densitogram intensity is plotted versus multimer size in terms of dimer number  $i$ . (E) Fits of normalized data show no significant difference in size distribution between rVWF (gray squares) and fluorescent rVWF-eGFP (black squares), stressing that the recombinant distribution with fused eGFP exhibits a normal multimerization behavior. Best fits to the gel data are obtained using an exponential function  $N(i) = N_1 p^{i-1}$  with an extent of polymerization of  $p = 0.70$  (black dotted line). For pathological rVWF-IIC (green triangles), a reduced extent of polymerization of  $p = 0.36$  (dark green dotted line) for rVWF-IIC and  $p = 0.22$  (green dotted line) for rVWF-IIC-eGFP is obtained. (F) Both plasma samples show likewise an exponential decay with a decreased  $p = 0.66$  for pathological VWF-IIC (VWF-NP:  $p = 0.78$ ). We observe a small, systematic deviation for large multimer sizes due to enzymatic cleavage in the plasma.

Here,  $N_i$  and  $N$  represent the number of  $i$ -mers and the total number of VWF molecules, respectively.  $p$  indicates the extent of polymerization, i.e., the number of polymerized subunits to the total number of subunits,  $N$ . We assume that VWF multimerization complies with the step-growth polymerization model insofar as the formation of disulfide bonds can be assumed to be independent of size and the reaction volume is finite, which is a reasonable assumption considering the fact that multimerization occurs in the Golgi Apparatus only. Fitting the measured size distribution by the exponential function  $N(i) = N_1 p^{i-1}$  yields an extent of polymerization of  $p = 0.70 \pm 0.02$  for rVWF.  $N_1$  is a constant fitting parameter that contains information about the number of dimers available for polymerization (for details, see the Supporting Material).  $p$  describes the slope of the size distribution:

high values of  $p$  indicate a slowly decaying size distribution with long multimers being more abundant, whereas small values of  $p$  indicate a steep decay with only a small amount of long multimers. The same exponential decay as for rVWF is found for rVWF-eGFP (black squares), showing that the shape of the distribution does not change significantly when fusing eGFP to VWF. The recombinant VWF-eGFP construct is therefore well suited for further studies employing fluorescence microscopy. The pathological rVWF-IIC appears only in a few bands of short sizes due to its lack of large multimers. Fitting yields an exponential, as for physiological VWF, yet with an extent of polymerization  $p = 0.36 \pm 0.01$  for rVWF-IIC (dark green) and  $p = 0.22 \pm 0.01$  for rVWF-IIC-eGFP (green).

Physiological VWF derived from blood samples also exhibits an exponential decrease (Fig. 2 F) with an extent of polymerization  $p = 0.78 \pm 0.02$  for normal patients. However, the distribution function seems to exhibit a slight, but systematic deviation underrepresenting the larger fraction. This deviation can be attributed to ADAMTS13-induced cleavage that occurs in plasma and is depicted in the gels by the two satellite bands flanking the main bands that are known to be the products of proteolysis. Pathological VWF-IIC from plasma of patients suffering from von Willebrand disease type IIC shows an extent of polymerization  $p = 0.66 \pm 0.01$ .

### FCS single-component analysis of rVWF

FCS allows for size measurements of fluorescently labeled VWF in solution and is in principle capable to resolve multiple species with varying diffusion properties. We find that the measured FCS autocorrelation functions of recombinant VWF-eGFP are consistent with an exponential size distribution. First, we investigate recombinant VWF-eGFP (rVWF) monomer and dimer. A single-component analysis provides diffusion times (diffusion coefficients) of  $\tau_D = 322 \mu\text{s}$  ( $D = 31.9 \mu\text{m}^2/\text{s}$ ) for the monomer and  $\tau_D = 447 \mu\text{s}$  ( $D = 19.5 \mu\text{m}^2/\text{s}$ ) for the dimer (Fig. 3 A). Fig. 3 A also shows purified eGFP as a control. The eGFP diffusion time of  $\tau_D = 90 \mu\text{s}$  is in agreement with previous results (37). Because VWF is a rather elongated protein (11) a crude approximation of the VWF monomer and the VWF dimer as cylinders with the same diameter and twice the length for the dimer is reasonable. With these assumptions, the measured diffusion coefficients correspond to a cylinder 3 nm in diameter and 85.3 nm (dimer) and 42.7 nm (monomer) in length (for details, see the Supporting Material). This is in accordance with experiments performed by tapping mode atomic force microscopy (38) and electron microscopy measurements (11).

The single-component analysis can also be used as a first approximation of the full VWF distribution. Because it averages over all the species within the sample, it cannot

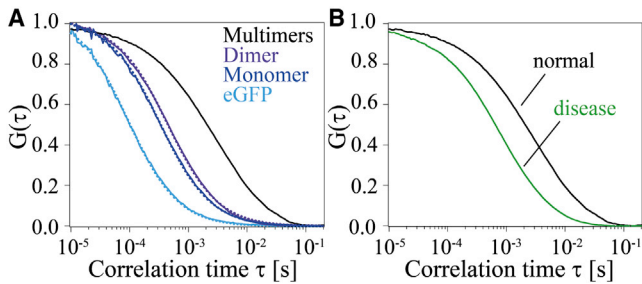


**FIGURE 3** FCS measurements of recombinant VWF distributions and their building blocks. (A) Single-component fits of eGFP (light blue), rVWF monomer (dark blue), and rVWF dimer (purple) give correlation times  $\tau_D$  of 90  $\mu$ s, 322  $\mu$ s, and 447  $\mu$ s. Assuming a cylindrical shape for the dimer, the corresponding diffusion coefficient  $D = 19.5 \mu\text{m}^2/\text{s}$  characterizes a cylinder with length  $l = 85.3 \text{ nm}$  and  $d = 3 \text{ nm}$ . A clear shift toward longer diffusion times can be seen for the multimer distribution rVWF (black). (B) Single-component analysis was used as a first estimate of the autocorrelation function of physiological rVWF (black). A clear shift can be seen for pathological rVWF-IIC (green) that allows distinguishing between normal and abnormal conditions. Average diffusion times of  $\tau_D = 2244 \pm 515 \mu\text{s}$  (rVWF) and  $\tau_D = 712 \pm 22 \mu\text{s}$  (rVWF-IIC) are obtained.

reflect the different species within the VWF size distribution. Thus, single-component analysis is not able to provide the actual size distribution  $N(i)$ . However, it provides an average VWF size and is suited to rapidly pinpoint differences between the physiological distribution of rVWF and of the pathological distribution rVWF-IIC (Fig. 3 B) showing an average diffusion time of  $\tau_D = 2244 \pm 515 \mu\text{s}$  (black line) for physiological and  $\tau_D = 712 \pm 22 \mu\text{s}$  (green line) for pathological rVWF. For rVWF, the diffusion time is in good agreement with measurements performed by Torres et al. (39) who detected an average diffusion time of 2.0–3.5 ms for VWF-NP bound to fluorescently labeled antibodies. For rVWF-IIC, the lack of large multimers explains the shift to shorter diffusion times in our measurements. Although this single-component analysis does not contain quantitative information about the size distribution of VWF, it is clearly sufficient to distinguish between the physiological and the investigated pathological VWF distribution (Fig. 3 B).

### FCS multicomponent analysis of rVWF

To examine the nature of the VWF size distribution a multimer analysis was applied (Fig. 4) and found to be consistent with the exponential size distribution measured with quantitative gel analysis. The multimer analysis allows to compare the autocorrelation function expected for a given size distribution  $N(i)$  with the experimental autocorrelation curve (see the Supporting Material, S1). Several distribution functions were tested for  $N(i)$ . Best results are achieved using an exponential function  $N(i) = N_1 p^{i-1}$  in agreement with the data obtained with quantitative gel analysis. The base is found to be  $p = 0.64$  for physiological rVWF (Fig. 4 A) and  $p = 0.18$  for pathological rVWF-IIC (Fig. 4 B).

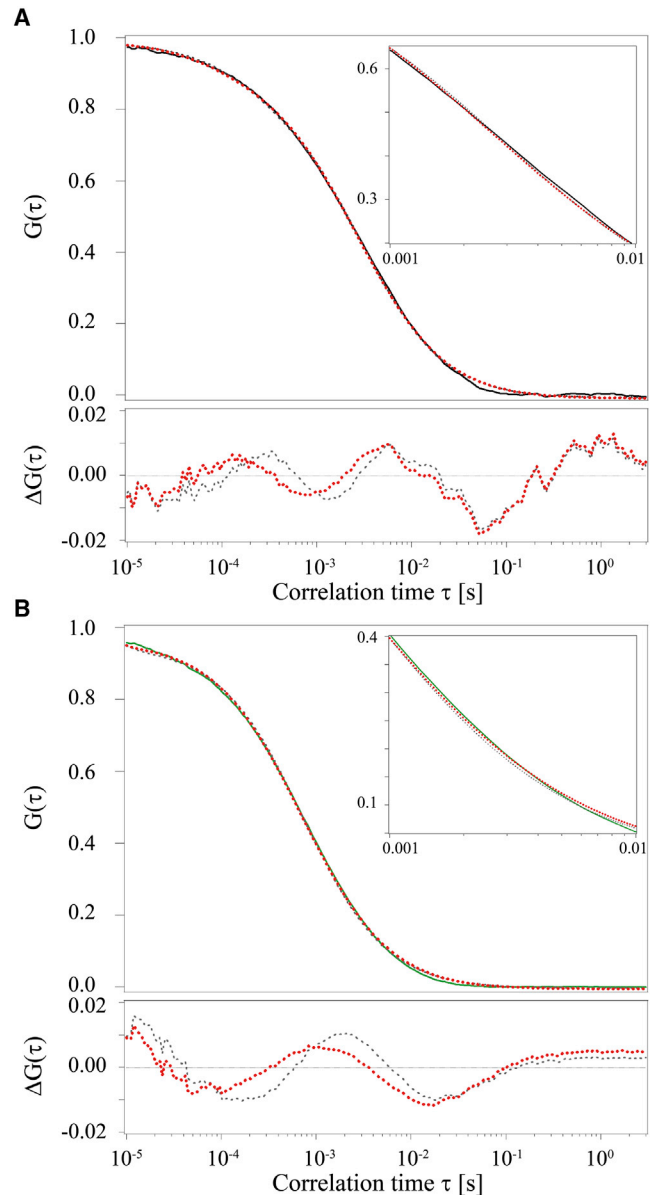


**FIGURE 4** Multimer analysis of rVWF using FCS. (A) Multicomponent fit (red dotted line) of the autocorrelation function of physiological rVWF (black line) leads to a size distribution that decays with the base  $p = 0.64$ . Furthermore, the single-component analysis (gray dashed line) fits the distribution well, yielding an average multimer size of  $\bar{i} = 6.3 \pm 1.4$  dimers. (B) With the multicomponent fit (red dotted line) for the pathological distribution rVWF-IIC (green line), the base is determined to be  $p = 0.18$ , indicating the lack of large VWF multimers. Single-component fit (gray dashed line) infers an average multimer size of  $\bar{i} = 2.0 \pm 0.1$  dimers.

The best fit to the exponential distribution shows a small improvement over the initial single component analysis (Fig. 4). The fact that the multicomponent analysis is close to a single component fit is explained by the fact that the FCS autocorrelation function weights each molecule with its squared brightness (see the Supporting Material). For rVWF-eGFP the brightness scales with the number of dimers  $i$ , the resulting weighted size distribution

is  $N'(i) = i^2 N(i)$ , which exhibits a sharp maximum at the average multimer size  $\bar{i} = 4.7$ . Due to the narrow weighted distribution function, the multicomponent fit appears to be close to the fit of a single species. The average multimer size is in good agreement with the average multimer size obtained with single-component analysis that yields  $\bar{i} = 6.3 \pm 1.3$  for rVWF (for details see the [Supporting Material S1](#)). For the mutant rVWF-IIC with  $p = 0.18$ , an average multimer size of  $\bar{i} = 1.5$  is calculated compared to  $\bar{i} = 2.0 \pm 0.1$  measured with the single-component fit. However, it is important to note that the proper multicomponent analysis using the proposed exponential size distribution  $N(i)$  describes the measured autocorrelation function the best within the experimental accuracy.

### Direct imaging of VWF with TIRFM

The data presented so far reveals an exponential size distribution of VWF. Using TIRFM, we confirmed these results by direct imaging. Under continuous excitation, the fluorescence signal of rVWF-eGFP was observed to decrease in discrete steps over time. As described in (40) and explained in detail in the [Supporting Material S3](#), the number of bleaching steps can be taken as a measure for the number of eGFP-tagged VWF monomers. Counting bleaching steps therefore provides a means for analyzing the VWF size distribution. Measurements of an rVWF dimer sample proved that this analysis method is indeed suitable for our samples (see the [Supporting Material S3](#)).

For localizing the rVWF multimers, an average image of the first 100 frames was calculated (Fig. 5 A) and regions of interest were selected. Bleaching steps in the intensity-time traces of these regions were identified with the step detection algorithm described in (41) (Fig. 5, B and C). The relative frequency for detecting a certain number of steps was plotted versus the number of steps (Fig. 5 D) and each step number was assigned to a certain multimer size. As we count the multimer size in number of dimers  $i$  but the bleaching steps scale with the number of monomers, two bleaching steps add up to an increase of one in the multimer size. Odd numbers of bleaching steps were round up to the next even number. The thereby obtained size distribution  $N(i)$  was plotted versus the multimer size in number of dimers  $i$ . Fitting yields an exponentially decaying size distribution  $N(i) = N_1 p^{i-1}$  with a base  $p = 0.29$  (Fig. 5 D), convincingly confirming the findings from quantitative gel analysis and FCS.

### Effect of ADAMTS13 cleavage on VWF size distribution

The VWF size distribution is after secretion into the blood plasma dynamically controlled by the protease ADAMTS13 (Fig. 1 D) with defects in ADAMTS13 activity resulting in unusually large VWF that cause thrombotic thrombocyto-

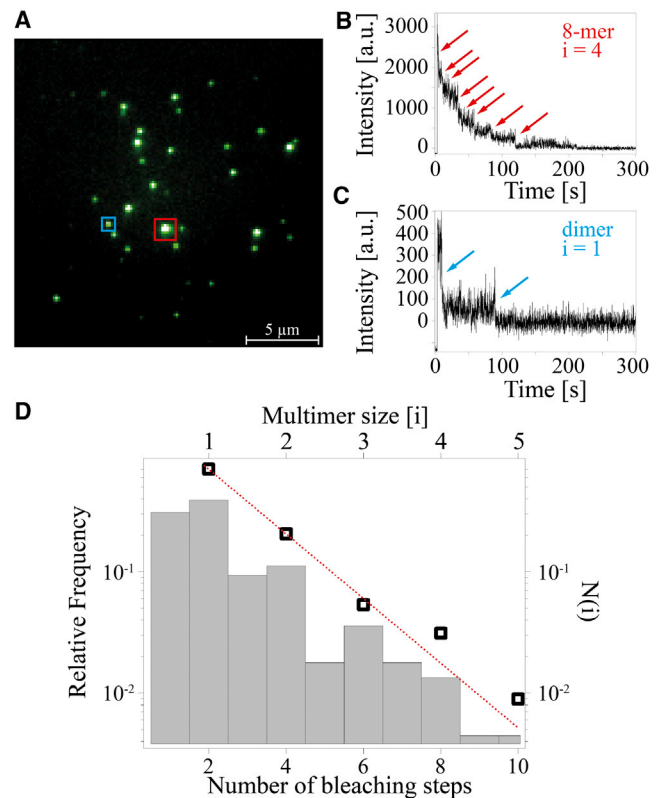
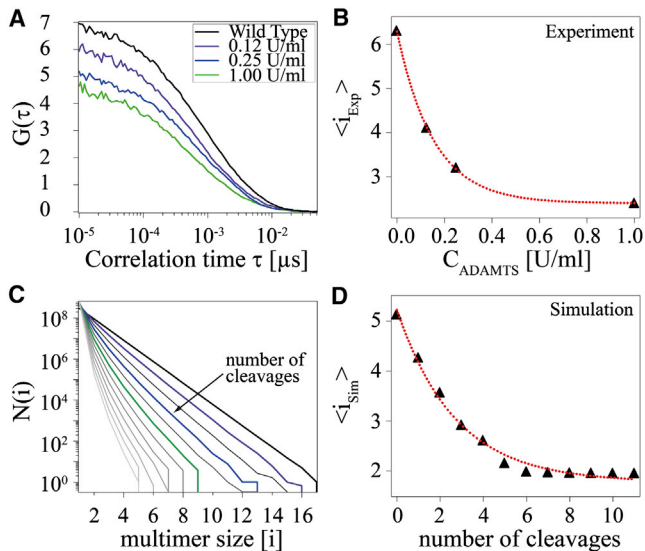


FIGURE 5 Direct imaging of rVWF using TIRFM. (A) TIRFM image of VWF multimers immobilized on a glass surface. The multimer size is determined by counting eGFP bleaching steps as each rVWF monomer is labeled with one eGFP. The intensity-time traces of the two highlighted molecules represent an 8-mer (B) and a dimer (C). The positions of the counted steps are indicated with arrows. (D) The relative frequency for detecting a certain number of steps in the intensity trace is shown as a bar chart. Size distribution analysis of  $N(i)$  (black squares) yields, in good agreement with the results from quantitative gel analysis and FCS, an exponentially decaying size distribution  $N(i) = N_1 p^{i-1}$  (red dots) with the base  $p = 0.29$ .

penic purpura. We investigated this time-dependent evolution of the VWF size distribution with FCS and found systematic shifts to smaller multimer sizes that are no longer exponentially distributed. Various concentrations of ADAMTS13 were used to visualize different cleavage states. rVWF concentrated to 65% of normal plasma concentration (0.65 units/ml) was digested by 0.12, 0.25, and 1.00 units/ml ADAMTS13. As expected, the cleavage due to ADAMTS13 shifts the autocorrelation curves to higher particle numbers (lower amplitude) and shorter diffusion times (steeper decay). It is not possible to describe these autocorrelation curves with a multicomponent analysis with an exponentially decaying size distribution  $N(i)$ , indicating that the cleavage changes the shape of the distribution. Yet, using single-component analysis it is possible to extract average diffusion times of  $\tau_D = 1045 \mu\text{s}$ ,  $813 \mu\text{s}$ , and  $617 \mu\text{s}$  (0.12, 0.25 and 1.00 units/ml ADAMTS13) (Fig. 6 A). We find an exponential dependence of the average multimer size in terms of dimer number  $i$  on the



**FIGURE 6** Multimer analysis after ADAMTS13-induced proteolytic cleavage. (A) Varying concentrations of ADAMTS13 are used to visualize different cleavage states. Correlation curves of rVWF distribution are shifted toward lower correlation times and higher particle concentrations (lower  $G(0)$ ) with increasing protease concentration. (B) Single-component analysis indicates an exponential decay of the average multimer sizes with increasing ADAMTS13 concentration. (C) Simulation of a random cleavage process shows the changes in the size distribution due to ADAMTS13 cleavage. (D) Average multimer sizes decrease exponentially with an increasing number of cleavage steps per molecule. Comparing the decay constant in (B) and (D),  $\sim 0.1$  units/ml ADAMTS13 and one cleavage step per molecule lead to a similar effect on the average multimer size.

ADAMTS13 concentration with  $\bar{i} = 4.5, 2.6,$  and  $1.2,$  corresponding to  $0.12, 0.25,$  and  $1.00$  units/ml concentration of ADAMTS13 (Fig. 6 B).

To get an estimate of the size distribution in the presence of ADAMTS13, the cleavage process was simulated based on a model that assumes random cleavage sites combined with equal cleavage probability for all multimer sizes (Fig. 6 C). Starting with the measured exponentially shaped multimer distribution, each iteration cuts each multimer once at a random site. For each iteration, the average multimer size of the generated size distribution is calculated and plotted against the number of cleavage steps (Fig. 6 D). Comparison of experiment and simulation (Fig. 6, C and D), shows that the average multimer size scales exponentially with the number of cleavages of each molecule, with  $\sim 0.1$  units/ml ADAMTS13 and one cleavage step resulting in the same average multimer size. This means that a  $0.1$  units/ml ADAMTS13 concentration is necessary to cleave each molecule of a  $0.65$  units/ml VWF concentration once within  $5$  h.

## DISCUSSION

In this article, we found independent evidence that the size of recombinant VWF is exponentially distributed. First

quantitative gel analysis of VWF based on antibody staining indicates an exponential size distribution, second a FCS multicomponent analysis of recombinant VWF-eGFP proves consistent with the proposed distribution function, and finally the frequency distribution obtained from direct single molecule fluorescence imaging yields an exponential dependence for the first five VWF-eGFP multimer sizes. An exponential size distribution as such is not unexpected and well known for both equilibrium polymers (42) and linear condensation polymers (8). An equilibrium polymer forms by reversible association of subunits with mutual binding constant affinity. Prominent examples for equilibrium polymers are actin, microtubulin, and other cytoskeleton filaments (43). Linear condensation polymers are formed by irreversible growth mechanisms. It is well established that VWF is a covalently linked multimer as the VWF multimerization occurs via formation of disulfide bonds. Furthermore, it is understood that the VWF multimerization takes place in the Golgi, where the propeptide of VWF itself acts as oxidoreductase, thereby facilitating disulfide bond formation that allows VWF to polymerize in this compartment (12–14). An exponential size distribution results if the reactivity of subunits is independent of the segment size and takes place in a finite compartment. In this case, the molar fraction of segments containing  $i$  subunits is given by Eq. 1. The distribution is fully determined by a single parameter, the extent of polymerization,  $p$ . This extent of polymerization is limited both by the reaction rate of the VWF molecules to each other and by the reaction time, which is determined by the time the VWF remains in the Golgi. We find that the fraction of polymerized dimers is  $p_{rVWF} = 0.70 \pm 0.02$  for rVWF and  $p_{rVWF-IIC} = 0.22 \pm 0.01$  in case of the pathological form rVWF-IIC. It is noteworthy that for the disease mutant VWF-IIC, the exponentially decaying size distribution is maintained indicating that the mechanism of biosynthesis is the same. As aberrances in the size distribution of VWF-IIC are caused by mutations in the VWF propeptide that prevent multimerization in the Golgi (44), a decreased reaction rate can be assumed and explains the lower extent of polymerization.

The fact that the exponential VWF size distribution is in accordance with a step-growth reaction mechanism allows the quantification of a VWF distribution by a single parameter. Knowing the extent of polymerization  $p$  yields the entire range of multimers. An interesting finding is the fact that the extent of polymerization is in general fairly low with far less long multimers being formed than hitherto expected. For the physiological distribution rVWF, 30% of VWF dimers remain as non-polymeric species. Multimers consisting of five or more dimers account for only 24% of the total number of VWF molecules whereas multimers containing 10 or more dimers represent just 4%. Hence, the polymeric form of VWF that is supposed to be the one most relevant for VWF function is a minority species of VWF. Secondly, as characteristic for the base of an

exponential function, already small changes in  $p$  have a strong leverage on the multimer distribution and consequently a detrimental impact on the physiological state. A loss of 25% in the extent of polymerization reduces the number of 10mers by a factor of 100.

The size distribution of VWF is changed upon secretion to the blood plasma by ADAMTS13-induced cleavage. We used rVWF to mimic this cleavage process. Varied cleavage states represented by different concentrations of ADAMTS13 can be clearly distinguished from uncleaved rVWF. The exponentially shaped size distribution is not maintained during cleavage. Simulation of a random cleavage process allows us to relate the ADAMTS13 concentration to a certain number of cleavage steps. We show that cleavage with 0.1 units/ml ADAMTS13 concentration under partly denaturing condition in urea has the same effect on the average multimer size as cutting each VWF molecule once at a random site. In blood plasma, ADAMTS13-induced cleavage is assumed to require shear-induced stretching of VWF. We find that the size distribution of healthy patients exhibits almost the same exponential size dependence as recombinantly expressed VWF. Small deviations at larger size fractions could be indicative of extracellular ADAMTS13 activity in blood flow. Interestingly, the size distribution of patients exhibiting von Willebrand disease type IIC showed less deviation from the normal case as predicted from the recombinant expressed VWF-IIC. It must be assumed that the deficiency in the extent of polymerization is partly compensated, possibly by VWF expelled from Weibel-Palade bodies. Plasma VWF is essential for the initiation of blood coagulation but is immediately joined by VWF stored in the granules of endothelium cells (Weibel-Palade bodies) at the beginning of hemostasis so that long VWF multimers can be provided whenever needed.

From a measurement technique point of view, we showed that FCS is capable of following the evolution of VWF size distribution under blood plasma conditions. This opens up the possibility to use recombinant VWF-eGFP in combination with FCS as a diagnostic assay for ADAMTS13 activity in hematology. Moreover, FCS has the capability to use shear forces during measurement. Therefore, experiments with urea as a stretcher could become redundant and be replaced by measurements under shear flow in situ.

## CONCLUSION

In this work, we reported on the exponential size distribution of recombinant and physiological VWF multimers. We found evidence that the exponential distribution is the generic outcome of VWF biosynthesis as disease-related VWF mutant VWF-IIC also exhibits an exponential size distribution, albeit with a smaller extent of polymerization. In light of this finding, we hypothesize that the disease-related mutation type IIC affects the polymerization reac-

tion. We show that FCS allows for monitoring the change in VWF-eGFP size distribution under blood plasma conditions over time. In particular, ADAMTS13 activity was measured and it was shown that the decreasing average VWF size is in agreement with the expected evolution of an exponential distribution under random cleavage. We believe that the extent of polymerization, describing the size distribution of VWF, provides a valuable indicator in VWF-related disease diagnostics and that FCS proves valuable as a quantitative tool to follow the evolution of VWF size distribution in vitro over time.

## SUPPORTING MATERIAL

Two figures, supporting analysis, and references (45,46) are available at [http://www.biophysj.org/biophysj/supplemental/S0006-3495\(13\)00859-X](http://www.biophysj.org/biophysj/supplemental/S0006-3495(13)00859-X).

We thank Hanna Engelke for fruitful discussions and reading the manuscript. Mathias Strackharn and Stephan Heucke are gratefully acknowledged for their support with the TIRFM setup.

This work was supported with seed funds from the Center for NanoScience and the priority network within the Deutsche Forschungsgemeinschaft SHENC (Shear Flow Regulation of Hemostasis - bridging the gap between Nanomechanics and Clinical presentation), DFG research unit FOR 1543. We thank all SHENC members, especially Maria A. Brehm. S.L. thanks the support by the Elite Network of Bavaria.

## REFERENCES

- Sadler, J. E. 1998. Biochemistry and genetics of von Willebrand factor. *Annu. Rev. Biochem.* 67:395–424.
- Ruggeri, Z. M. 2001. Structure of von Willebrand factor and its function in platelet adhesion and thrombus formation. *Best Pract. Res. Clin. Haematol.* 14:257–279.
- Ruggeri, Z. M. 1997. von Willebrand factor. *J. Clin. Invest.* 99:559–564.
- Furlan, M., R. Robles, and B. Lämmle. 1996. Partial purification and characterization of a protease from human plasma cleaving von Willebrand factor to fragments produced by in vivo proteolysis. *Blood.* 87:4223–4234.
- Siedlecki, C. A., B. J. Lestini, ..., R. E. Marchant. 1996. Shear-dependent changes in the three-dimensional structure of human von Willebrand factor. *Blood.* 88:2939–2950.
- Schneider, S. W., S. Nuschele, ..., M. F. Schneider. 2007. Shear-induced unfolding triggers adhesion of von Willebrand factor fibers. *Proc. Natl. Acad. Sci. USA.* 104:7899–7903.
- Zhang, X., K. Halvorsen, ..., T. A. Springer. 2009. Mechanoenzymatic cleavage of the ultralarge vascular protein von Willebrand factor. *Science.* 324:1330–1334.
- Flory, P. J. 1936. Molecular size distribution in linear condensation polymers. *J. Am. Chem. Soc.* 58:1877–1885.
- Wagner, D. D. 1990. Cell biology of von Willebrand factor. *Annu. Rev. Cell Biol.* 6:217–246.
- Singh, I., H. Shankaran, ..., S. Neelamegham. 2006. Solution structure of human von Willebrand factor studied using small angle neutron scattering. *J. Biol. Chem.* 281:38266–38275.
- Springer, T. A. 2011. Biology and physics of von Willebrand factor concatamers. *J. Thromb. Haemost.* 9 (Suppl 1):130–143.
- Wise, R. J., D. D. Pittman, ..., S. H. Orkin. 1988. The propeptide of von Willebrand factor independently mediates the assembly of von Willebrand multimers. *Cell.* 52:229–236.

13. Purvis, A. R., and J. E. Sadler. 2004. A covalent oxidoreductase intermediate in propeptide-dependent von Willebrand factor multimerization. *J. Biol. Chem.* 279:49982–49988.
14. Dang, L. T., A. R. Purvis, ..., J. E. Sadler. 2011. Phylogenetic and functional analysis of histidine residues essential for pH-dependent multimerization of von Willebrand factor. *J. Biol. Chem.* 286:25763–25769.
15. McCarroll, D. R., E. G. Levin, and R. R. Montgomery. 1985. Endothelial cell synthesis of von Willebrand antigen II, von Willebrand factor, and von Willebrand factor/von Willebrand antigen II complex. *J. Clin. Invest.* 75:1089–1095.
16. Fay, P. J., Y. Kawai, ..., V. J. Marder. 1986. Propolypeptide of von Willebrand factor circulates in blood and is identical to von Willebrand antigen II. *Science.* 232:995–998.
17. de Wit, T. R., and J. A. van Mourik. 2001. Biosynthesis, processing and secretion of von Willebrand factor: biological implications. *Best Pract. Res. Clin. Haematol.* 14:241–255.
18. Tsai, H. M. 1996. Physiologic cleavage of von Willebrand factor by a plasma protease is dependent on its conformation and requires calcium ion. *Blood.* 87:4235–4244.
19. Gaucher, C., J. Diéval, and C. Mazurier. 1994. Characterization of von Willebrand factor gene defects in two unrelated patients with type IIC von Willebrand disease. *Blood.* 84:1024–1030.
20. Schneppenheim, R., K. B. Thomas, ..., B. Zieger. 1995. Identification of a candidate missense mutation in a family with von Willebrand disease type IIC. *Hum. Genet.* 95:681–686.
21. Schneppenheim, R., J. J. Michiels, ..., U. Budde. 2010. A cluster of mutations in the D3 domain of von Willebrand factor correlates with a distinct subgroup of von Willebrand disease: type 2A/IIe. *Blood.* 115:4894–4901.
22. Schneppenheim, R., H. Plendl, and U. Budde. 1988. Luminography—an alternative assay for detection of von Willebrand factor multimers. *Thromb. Haemost.* 60:133–136.
23. Budde, U., R. Schneppenheim, ..., I. Peake. 2008. Detailed von Willebrand factor multimer analysis in patients with von Willebrand disease in the European study, molecular and clinical markers for the diagnosis and management of type 1 von Willebrand disease (MCMDM-1VWD). *J. Thromb. Haemost.* 6:762–771.
24. Magde, D., E. Elson, and W. W. Webb. 1972. Thermodynamic fluctuations in a reacting system—measurement by fluorescence correlation spectroscopy. *Phys. Rev. Lett.* 29:705–708.
25. Elson, E. L., and D. Magde. 1974. Fluorescence correlation spectroscopy. I. Conceptual basis and theory. *Biopolymers.* 13:1–27.
26. Magde, D., E. L. Elson, and W. W. Webb. 1974. Fluorescence correlation spectroscopy. II. An experimental realization. *Biopolymers.* 13:29–61.
27. Rigler, R., Ü. Mets, ..., P. Kask. 1993. Fluorescence correlation spectroscopy with high count rate and low background: analysis of translational diffusion. *Eur. Biophys. J.* 22:169–175.
28. Petrov, E. P., and P. Schwill. 2008. State of the art and novel trends in fluorescence correlation spectroscopy. In *Standardization and Quality Assurance in Fluorescence Measurements II*. U. Resch-Grenger, editor. Springer, pp. 145–197.
29. Thompson, N. L. 1991. Fluorescence correlation spectroscopy. In *Topics in Fluorescence Spectroscopy*, Vol. 1. J. R. Lakowicz, editor. Plenum Press, New York, pp. 337–378.
30. Engelke, H., I. Dorn, and J. O. Rädler. 2009. Diffusion and molecular binding in crowded vesicle solutions measured by fluorescence correlation spectroscopy. *Soft Matter.* 5:4283–4289.
31. Zanardelli, S., A. C. K. Chion, ..., D. A. Lane. 2009. A novel binding site for ADAMTS13 constitutively exposed on the surface of globular VWF. *Blood.* 114:2819–2828.
32. Alkaabi, K. M., A. Yafea, and S. S. Ashraf. 2005. Effect of pH on thermal- and chemical-induced denaturation of GFP. *Appl. Biochem. Biotechnol.* 126:149–156.
33. Axelrod, D. 1981. Cell-substrate contacts illuminated by total internal reflection fluorescence. *J. Cell Biol.* 89:141–145.
34. Kufer, S. K., M. Strackham, ..., H. E. Gaub. 2009. Optically monitoring the mechanical assembly of single molecules. *Nat. Nanotechnol.* 4:45–49.
35. Gump, H., S. W. Stahl, ..., H. E. Gaub. 2009. Ultrastable combined atomic force and total internal fluorescence microscope. *Rev. Sci. Instrum.* 80:063704–063705.
36. Pruss, C. M., C. R. P. Notley, ..., D. Lillicrap. 2008. ADAMTS13 cleavage efficiency is altered by mutagenic and, to a lesser extent, polymorphic sequence changes in the A1 and A2 domains of von Willebrand factor. *Br. J. Haematol.* 143:552–558.
37. Petrásek, Z., and P. Schwill. 2008. Precise measurement of diffusion coefficients using scanning fluorescence correlation spectroscopy. *Biophys. J.* 94:1437–1448.
38. Seyfried, B. K., G. Friedbacher, ..., P. L. Turecek. 2010. Comparison of plasma-derived and recombinant von Willebrand factor by atomic force microscopy. *Thromb. Haemost.* 104:523–530.
39. Torres, R., J. R. Genzen, and M. J. Levene. 2012. Clinical measurement of von Willebrand factor by fluorescence correlation spectroscopy. *Clin. Chem.* 58:1010–1018.
40. Ulbrich, M. H., and E. Y. Isacoff. 2007. Subunit counting in membrane-bound proteins. *Nat. Methods.* 4:319–321.
41. Opfer, J., and K.-E. Gottschalk. 2012. Identifying discrete states of a biological system using a novel step detection algorithm. *PLoS ONE.* 7:e45896.
42. Hill, T. L. 1987. *Linear aggregation theory in cell biology*. Springer-Verlag, New York.
43. Howard, J. 2001. *Mechanics of motor proteins and the cytoskeleton*. Sinauer Associates, Sunderland, MA.
44. Sadler, J. E., U. Budde, ..., A. B. Federici; Working Party on von Willebrand Disease Classification. 2006. Update on the pathophysiology and classification of von Willebrand disease: a report of the Subcommittee on von Willebrand Factor. *J. Thromb. Haemost.* 4:2103–2114.
45. Rouse, Jr., P. E. 1953. A theory of the linear viscoelastic properties of dilute solutions of coiling polymers. *J. Chem. Phys.* 21:1272–1280.
46. Inoué, S., O. Shimomura, ..., P. T. Tran. 2002. Fluorescence polarization of green fluorescence protein. *Proc. Natl. Acad. Sci. USA.* 99:4272–4277.